

# Simonkolleite-graphene foam composites and their superior electrochemical performance

D.Y. Momodu, F. Barzegar, B. Abdulhakeem, J. Dangbegnon, T. Masikhwa, J. Madito and N. Manyala\*

Department of Physics, Institute of Applied Materials, SARCHI Chair in Carbon Technology and Materials,  
University of Pretoria, Pretoria 0028, South Africa.

\*Corresponding author. E-mail address: [ncholu.manyala@up.ac.za](mailto:ncholu.manyala@up.ac.za), Tel.: +27 012 420 3549; Fax: +27 012 420 2516

(N. Manyala)

## Abstract

Simonkolleite-graphene foam (SimonK/GF) composite has been synthesized by a facile solvothermal and environmentally friendly technique with excellent electrochemical properties. The obtained product was initially analyzed by scanning electron microscopy (SEM), Brunauer–Emmett–Teller (BET), X-ray diffraction (XRD), Fourier transform infrared resonance (FTIR) spectroscopy and cyclic voltammetry (CV) techniques. The microscopy results reveal hexagonal sheets interlaced with each other and adjacent graphene sheets. The existence of graphene foam in the simonK/GF composite is further confirmed from the structural and the optical characteristics obtained from XRD and FTIR respectively. The BET results obtained indicate an improvement in the surface area due to the addition of graphene foam to a value of  $39.58 \text{ m}^2 \text{ g}^{-1}$ . The  $\text{N}_2$  adsorption/desorption also shows the presence of active mesopores required for charge transport. As a promising electrode material for supercapacitors, the composite shows a high specific capacitance value of  $1094 \text{ F/g}$  at  $1 \text{ A/g}$  with a coulombic efficiency of 100% after 1000 cycles. These results show a potential for adoption of this composite in energy storage applications.

**KEYWORDS:** *simonkolleite sheets, graphene foam, composites, supercapacitor*

## 1. Introduction

In the developing field of energy storage technology, the design and fabrication of efficient energy storage devices with high energy and power densities are of growing concern today. Numerous scientists have engaged in active research to develop robust and reliable energy storage systems which will match the increasing demand for energy in a variety of applications from energy storage systems in portable hand-held devices to back-up systems in hybrid electric motor vehicles.

Supercapacitors (SCs) with high power densities and long cycle life as compared to much common hybrid batteries in use today are promising candidates for such applications. However, they are also characterized with low energy densities in comparison to batteries which creates a drawback for their wide applications [1]. The nature of the electrode material which makes up the SC is one of the most important factors that determine its performance.

Based on the device operation mechanism, SCs can be broadly divided into two classes; the electric double layer capacitors (EDLCs) and the pseudocapacitors [2]. In order to deal with the problem of low energy density, most recent studies include combining materials with pseudocapacitive and electric double layer capacitive (EDLC) properties [2–8]. This is achieved by combining high specific surface area carbonaceous materials (e.g. graphene [3,4], carbon nanotubes [5–7], activated carbon [8,9]) with transition metal oxides and hydroxides with good redox properties.

For example, Gao's research group illustrated the production of graphene nanosheet-layered double hydroxide (GNS/LDH) by a simple hydrothermal technique [3]. In the study, glucose was used as a reducing agent in place of toxic hydrazine to exfoliate graphene oxide (GO) and obtain

an even dispersion of GNS in water. The observed remarkable specific capacitance was attributed to be due to the combination of electric double layer capacitance (EDLC) and Faradaic pseudocapacitance from the open structure system with improved contact between the electrode/electrolyte interface [3]. The conductive network of graphene sheets overlapping each other was reported to facilitate fast electron transfer between the active composite material and the charge collector. Another study by Fao et al., [8] reports a graphene/MnO<sub>2</sub> composite as positive electrode synthesized by microwave irradiation with activated carbon nanofibres (ACN) as negative electrode in an asymmetrical cell with Na<sub>2</sub>SO<sub>4</sub> aqueous electrolyte. A maximum energy density of 51.1 Wh Kg<sup>-1</sup> at a corresponding power density of 102.2 W kg<sup>-1</sup> was obtained with excellent cycling stability retention of 97% after 1000 cycles. The observed device performance was attributed to the synergistic properties of both electrodes which provided an extended voltage window necessary for an improved energy density.

Recently, simonkolleites (SimonK, also known as zinc chloride hydroxide monohydrate, Zn<sub>5</sub>(OH)<sub>8</sub>Cl<sub>2</sub>·H<sub>2</sub>O) have received enormous attention due to their morphological properties composed of slabs and platelets suitable for numerous applications ranging from gas sensing [10] to materials for supercapacitor applications [11]. They also crystallize hexagonally with a perfect cleavage parallel to the (001) direction [12]. Similar to metal oxides, simonkolleites contain electrochemically active sites necessary for efficient charge storage. SimonK is electrically and chemically active due to the oxygen vacancies available on its surface, as in the case of ZnO. These vacancies may then act as n-type donors and subsequently improve the material's conductivity [10]. For supercapacitor applications, the abundance of a hexagonal microplatelet interactive network will likely provide the surface required for ionic surface interactions during operation. However, the pseudocapacitance of pristine simonK for energy storage is still low

when compared with other metal oxides and hydroxides due to their lower electrical conductivity, lower surface area and tendency of the sheets to stack together. To overcome such limitations, efforts have been made by previous researchers to use carbon materials, such as graphene [3,11] or surfactants [13], to reduce the restacking and also improve the sheet thickness which would consequently improve the surface area and active porous sites for charge transport and storage.

The obtained hybrid system composed of simonkolleite-graphene will most likely have an improved electron transport rate, high electrolyte contact area for ion accessibility by creating more pores within the composite material. The combination of the graphene foam with simonkolleite microplatelets integrates the positive properties of electric double layer capacitance and pseudocapacitance. In addition, an in situ solvothermal synthesis approach of the simonK in the presence of evenly dispersed graphene foam leads to the synthesis of a simonkolleite-graphene foam composite (SimonK/GF) electrode with successful delamination/spacing of the simonkolleite sheets and will subsequently produce thinner sheets with improved surface properties and specific capacitance [4,14]. The in situ growth approach on a conductive substrate such as nickel-foam graphene ensures the simplification of the entire fabrication process and the direct acquisition of the composite electrode for device application. Although these are the desired properties for energy storage nanomaterials suitable for supercapacitors applications, limited studies have been done in this regards in relation to simonkolleite microplatelets.

In this present study, based on the considerations mentioned above, the synthesis of simonkolleite-graphene foam composite (SimonK/GF) is carried out with a subsequent study on the morphological, structural and electrochemical properties of the synthesized product. Analysis

of the scanning microscopy images reveal relatively thin hexagonal sheets of simonkolleite interlaced with graphene sheets. Notably, the SimonK/GF composite showed an improved surface area with a superior electrochemical performance from cyclic voltammetry (CV) compared with SimonK alone. These results is a considerable improvement over earlier studies on simonkolleite structures for supercapacitor applications [11], wherein a similar in situ approach was adopted to grow simonkolleite on nickel foam-graphene template as electrode material for electrochemical applications. These results show the potential application of SimonK/GF composites as suitable electrodes for pseudocapacitors.

## **2. EXPERIMENTAL**

### **2.1. Synthesis of nickel foam-graphene template and graphene foam**

The nickel foam-graphene (NF-G) current collector was prepared by an atmospheric pressure chemical vapor deposition (AP-CVD) technique. Briefly, a known mass of compressed nickel foam template (Alantum, Munich, Germany), with an areal density of  $420 \text{ g m}^{-2}$  was placed in a quartz tube for the CVD growth of graphene. The nickel foam was first annealed at  $1000 \text{ }^\circ\text{C}$  in the presence of Ar and  $\text{H}_2$  gas for 60 minutes, prior to the introduction of the carbon source ( $\text{CH}_4$  gas) at  $968 \text{ }^\circ\text{C}$ . The flow rates of the gases Ar: $\text{H}_2$ : $\text{CH}_4$  were 300:200:10 SCCM respectively. After 60 minutes of deposition, the samples were rapidly cooled by manually pushing the quartz tube to a lower temperature region to obtain the nickel foam-graphene.

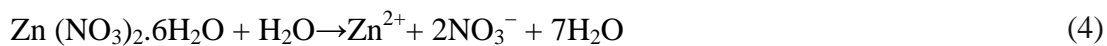
In order to obtain the graphene foam, the samples were further immersed in 3.0 M HCl and placed on a hot plate at  $60 \text{ }^\circ\text{C}$  to ensure complete etching of the nickel supporting structure. After

complete etching of the nickel, the remaining graphene foam was washed several times in deionized water and dried in the oven to obtain the final graphene foam product.

## 2.2. In situ synthesis of simonkolleite-graphene foam composite

Simonkolleite-graphene foam composite was deposited directly on the NF-G template using an aqueous chemical growth technique whereby a solution containing equimolar portions of 2.974g of zinc nitrate hexahydrate ( $\text{Zn}(\text{NO}_3)_2 \cdot 6\text{H}_2\text{O}$ ), 0.588g of sodium chloride (NaCl) and 4.102g of hexamethylenetetramine ( $\text{C}_6\text{H}_{12}\text{N}_4$ , HMT) were first dissolved in deionized water. The next step involved adding 25 mg of graphene foam sonicated for 12 hours in water to the mixture prepared earlier and stirring the combined mixture with graphene foam for 15 minutes. Subsequently, the final mixture was transferred into a 150 ml Teflon-lined autoclave vessel and nickel foam-graphene substrate were immersed vertically into the reaction vessel kept at 110 °C for 19 hours. Thereafter, the autoclave was allowed to gradually cool down to ambient temperature. The final simonK/GF composite electrode was obtained after washing and drying at 60 °C.

The formation of simonkolleite ( $\text{Zn}_5(\text{OH})_8\text{Cl}_2 \cdot \text{H}_2\text{O}$ ) proceeds competitively in the solution following a set of successive chemical reactions as reported in our earlier publication [11]:



Initially, HMT ( $C_6H_{12}N_4$ ) disintegrates into formaldehyde (HCHO) and ammonia ( $NH_3$ ). Ammonia tends to disintegrate deionized water to produce  $OH^-$  anions. Furthermore, NaCl disintegrates in water to form sodium cations ( $Na^+$ ) and (Cl) chloride anions while  $Zn(NO_3)_2 \cdot 6H_2O$  simultaneously disintegrates into zincate ( $Zn^{2+}$ ) and nitrate ( $NO_3^-$ ) ions. Lastly,  $OH^-$  and  $Cl^-$  anions react with  $Zn^{2+}$  cations to synthesize simonkolleite nanoplatelets ( $Zn_5(OH)_8Cl_2 \cdot H_2O$ ).

### **2.3. Material Characterization**

Scanning electron microscopy (SEM) analysis was carried out to reveal the morphology of the sample using a Zeiss Ultra Plus 55 field emission scanning electron microscope (FE-SEM) operated at an accelerating voltage of 2.0 kV. Surface area measurements were obtained using the Brunauer-Emmett-Teller (BET) method with  $N_2$  gas. Pore size and pore volume were obtained using Barrett-Joyner-Halenda (BJH) method from the desorption branch of the isotherm. The sample was also characterized using X-ray diffraction (XRD). An XPERT-PRO diffractometer (PANalytical BV, Netherlands) with theta/theta geometry, operating a cobalt tube at 35 kV and 50 mA, was used. The XRD patterns of all specimens were recorded in the  $10.0^\circ - 70.0^\circ 2\theta$  range with a counting time of 15.240 seconds per step. Qualitative phase analysis of the sample was conducted using the X'pert Highscore search match software. Fourier transform infrared (FT-IR) spectra of the SimonK were recorded using a Bruker Vertex 77v FT-IR spectrometer. The electrochemical properties were investigated using a Bio-Logic SP300 workstation (Knoxville TN 37930, USA) in a three-electrode configuration controlled by the EC-Lab® V10.37 software. The simonK/GF composite on NF-G served as the working electrode in

a 6.0 M potassium hydroxide (KOH) electrolyte; glassy carbon plate was used as the counter electrode and Ag/AgCl (3 M KCl) as the reference electrode.

The cyclic voltammetry tests were carried out in the potential range of 0 to 0.5 V (vs. Ag/AgCl) at different scan rates ranging from 10 to 100 mV s<sup>-1</sup>. The galvanostatic charge–discharge measurements were also carried out at different current densities from 1 to 10 A g<sup>-1</sup> and the electrochemical impedance spectroscopy (EIS) measurements were performed in the frequency range of 100 kHz–10 mHz.

### **3. Results and Discussion**

Fig. 1 shows the morphology of the in situ grown simonkolleite microplatelets with and without graphene foam obtained from microscopy analysis. Figs. 1a and b show the simonK sheets interlaced with each other at lower and higher magnifications respectively. Thinner microplatelets are obtained (shown by dashed-arrows in Figs. 1c and 1d at different magnification respectively) as a result of adding graphene foam to simonkolleite growth precursors which shows the successful exfoliation of the simonkolleite sheets with graphene flakes to form the simonK/GF composite. The average thickness of the pure simonK sheets is between 52 – 96 nm while the thickness is observed to reduce to about 30 – 45 nm for simonK/GF composite sheets. SimonK and simonK/GF interlaced sheets growing on the surface of a NF-G substrate are shown in Figs. 1e and f respectively. The combination of thin sheets of both simonkolleite and graphene is visible which is necessary for providing the surface required for charge transport and storage. The effect of the addition of graphene foam is clearly visible

from the thickness of the hexagonal sheets. The morphology observed from the microscopy images of the composite is ideal for electrochemical applications involving interface reactions.

The presence of a porous structure in the composite is confirmed from the Brunauer-Emmett-Teller (BET) method displayed in Fig. 2. Pore size distribution was obtained using Barrett-Joyner-Halenda (BJH) method from the desorption branch of the isotherm. The physical adsorption/desorption of N<sub>2</sub> at 77 K results are shown in Fig. 2a. The BET specific surface area (SSA) values for the simonK and simonK/GF composite were calculated to be 27.26 m<sup>2</sup> g<sup>-1</sup> and 39.58 m<sup>2</sup> g<sup>-1</sup> respectively. These values are comparable to or even larger than values reported in earlier research work on simonkolleite-based materials [15]. Fig. 2b shows the corresponding pore size distribution with a major pore diameter ranging from 2 - 4 nm which further confirms the presence of mesoporous sites which are used as pathways for transport of ions necessary for power delivery [16,17]. The supercapacitive performance of the active electrode material is dependent on its ability to accommodate as much active electrochemical sites for charge storage during operation. The presence of suitable mesopores within the electrode material is also ideal to ensure the reduction of mass transfer of electrolyte during fast redox reactions and facilitates power delivery [5].

Fig. 3a shows the XRD patterns of the synthesized simonK microplatelets and the composite electrode material with graphene foam added (simonK/GF). Typical diffraction peaks which correspond to the simonkolleite material are indexed to pure rhombohedra simonkolleite [Joint Committee on Powder Diffraction Standards (JCPDS No. 07-0155)]. These simonkolleite peaks are also similar to those reported in earlier studies [10,11] in which characteristic reflection patterns of the same material were studied. The sharp and strong peaks show the relatively high crystallinity of the sample. However, these peaks exhibit a shift due to the nature of the X-ray

source (cobalt) used in the analysis of the samples. For example, the reflection from the (003) plane with a strong diffraction peak usually ascribed to the  $2\theta$  angle of  $\sim 11.30^\circ$  [10] is now observed at  $15.10^\circ$ . Likewise, similar peak shifts exist for other planes, such as the (015), (110) and the graphene peak indexed as (002) plane which show diffraction peaks at  $2\theta$  values of  $28.00^\circ$ ,  $32.50^\circ$  and  $30.90^\circ$  respectively. The shifts are due to the difference in wavelength of the incoming X-rays which are dependent on the X-ray source, according to the Bragg equation  $n\lambda = 2d\sin\theta$ . In general, X-rays from a cobalt source ( $\lambda = 1.79 \text{ \AA}$ ) with longer wavelengths result in greater  $2\theta$  positions compared with those from a copper source ( $\lambda = 1.54 \text{ \AA}$ ). The former usually allows the observation of low-angle peaks that are not observable using the shorter wavelength X-rays and provides better peak separation [18]. The XRD analysis shows that simonkolleite has a strong preferential orientation along (003). The corresponding angular position of about  $2\theta_{(003)}$  which is  $\sim 15.10^\circ$  is related to the highly ordered reticular planes characterized by a  $d$ -spacing value of  $\sim 6.812 \text{ \AA}$  when calculated from the XRD data. The lattice constants for  $\langle a \rangle$  and  $\langle c \rangle$  are obtained as  $\sim 7.651 \text{ \AA}$  and  $\sim 20.435 \text{ \AA}$ , respectively.

Fig. 3b shows the FT-IR spectrum of the simonkolleite, simonkolleite-graphene foam composite and graphene foam (GF), respectively. These measurements were performed within a wavenumber range from 360 to  $3600 \text{ cm}^{-1}$ . A broad absorption band centered at about  $3435 \text{ cm}^{-1}$  corresponds to the O-H stretching vibrations of the interlayer water molecules [10,15]. The observed band at  $2358 \text{ cm}^{-1}$  is not observed in pure simonkolleite sample and is related to the presence of graphene foam (G\*) in the composite. This band is attributed to the C-H vibrations of the methylene group. Intensive bands at  $898 \text{ cm}^{-1}$  and  $719 \text{ cm}^{-1}$  are also observed and are due to stretching vibration modes of chloride (Cl<sup>-</sup>) ion [19,20]. The bands at approx.  $453 \text{ cm}^{-1}$  corresponds to translational modes of the Zn-O bonds [10].

Cyclic voltammetry (CV) measurements are used to understand the macroscopic electrochemical surface reactions at the electrode material during operation. Fig. 4a shows the CV curves for a NF-G current collector, simonkollite and simonkollite-graphene foam composite electrodes on the NF-G current collector at a scan rate of  $20 \text{ mV s}^{-1}$  in a potential window range of 0.0 - 0.5 V. The CV plots are characterized by symmetrical characteristic profiles that are well defined by cathodic (reduction reaction) and anodic (oxidation reaction) peaks [21]. This reveals that the electrode reaction corresponds to a quasi-reversible process, indicating that the measured capacitance in these materials is mainly based on the redox mechanism due to the pseudocapacitive behavior of the material [22]. The NF-G exhibited the lowest intensity current peaks due to the quasi-super hydrophobicity which is attributed to poor surface wetting leading to a reduced access to and limited utilization of the available surface area of pristine graphene [11]. It can also be clearly seen that the integral area of the CV graph of simonK/GF composite is the largest among the three materials in the plot, implying that it possesses the highest specific capacitance. The improved pseudocapitance could be due to the contributing effect from the added graphene foam which prevents the restacking of simonkollite sheets, thus producing thinner sheets with higher electrolyte ion ( $\text{K}^+$ ) accessibility and the highly conductive graphene layer on nickel foam.

Figs. 4b and 4c show the CV plot for simonK and simonK/GF composite in a potential window of 0.0 - 0.5 V at a scan rates ranging from 10 to  $100 \text{ mV s}^{-1}$ . The redox peaks are much precisely defined in the composite material compared to simonK alone. This is due to high thickness of the simonkollite platelets owing to aggregation, resulting in retarded transport of electrolyte ions [11]. On the other hand, for the composite electrode material containing graphene, the highly conductive sheets of graphene becomes entangled with the simonkollite platelets and provide

unobstructed pathways for  $K^+$  ion transport during the rapid charge–discharge process. The twin redox peaks are more visible in the composite material even at higher scan rates and are seen to undergo small shifts towards the left (negative potential) with increasing scan rate. The peaks at 0.39 V and 0.16 V are related to the anodic and cathodic peaks of the simonK/GF composite material at a scan rate of  $30 \text{ mV s}^{-1}$ . These peaks result from the intercalation and de-intercalation of  $K^+$  from the electrolyte into the  $Zn_5(OH)_8Cl_2 \cdot H_2O$  [11]. Thus the charge storage mechanism of simonkolleite-based composite electrodes is ascribed to the rapid intercalation of alkali metal cations  $K^+$  in the electrode during reduction and oxidation processes [11,23].

The galvanostatic charge–discharge curves for simonkolleite and simonkolleite-graphene foam composite were measured at different current densities of  $1.0 - 10.0 \text{ A g}^{-1}$  as shown in Figs. 4d and 4e respectively. The shape of the discharge curves shows a characteristic pseudocapacitance [24,25]; and this is in agreement with the CV curves which show redox peaks resulting from the oxidation-reduction reaction at the interface between the electrode and the electrolyte.

The specific capacitance was calculated from the galvanostatic discharge curves using the formula [5,26]:

$$C_s \text{ (F/g)} = I \times T_d / (m \times \Delta V) \quad (6)$$

where  $I$  is a current (A),  $T_d$  is the discharge time (s),  $m$  is the mass of active material (g), and  $\Delta V$  is the voltage range (V).

An enhancement in the discharge time for the simonK/GF composite electrode at  $1 \text{ A g}^{-1}$  current density is observed in Fig. 4e as compared with that of simonK alone (Fig. 4d). A specific capacitance of  $1094 \text{ F g}^{-1}$  is obtained for simonK/GF composite compared with a much lower specific capacitance value of  $741 \text{ F g}^{-1}$  for pristine simonK at a current density of  $1 \text{ A g}^{-1}$ . This is

a considerable enhancement and is a great improvement over our earlier studies on simonkolleite microplatelets prepared by an aqueous chemical growth method technique [11]. We therefore propose that the improvement in supercapacitance value is as a result of the addition of a porous and conducting graphene foam to the simonK matrix which provides an improved electron transfer rate and better structural support in form of exfoliation of thinner simonK microplatelets interacting with graphene sheets [11]. Fig. 4f shows the variation of the specific capacitance ( $C_s$ ) with current densities for both simonK and simonK/GF composite electrodes. From the figure, it can be observed that there is a decrease in specific capacitance with increasing current density. This is due to the limited movement of ions and protons by diffusion at higher current densities, which accesses only the outer active surface of the material for charge storage [5,27]

Fig. 5a shows the Nyquist plots obtained from the electrochemical impedance spectroscopy (EIS) measurements done at open circuit ( $E_{oc}$ ) potential to further evaluate the electrochemical behavior for the simonkolleite and simonkolleite-graphene foam composite at a frequency range of 10 mHz to 100 kHz. The scan begins from the high frequency (100 kHz) to the low frequency end (10 mHz). At the former frequency, a partial semi-circular arc is observed which is attributed to the dispersion effect [28]. At low frequency, the impedance plot should, theoretically, be a vertical line parallel to the vertical  $-Im(Z'')$  axis. However a slightly tilted vertical line is seen which indicates a pure capacitive behavior of the simonK material and low diffusion resistance of ions within the structure of the material [5]. The intersection of the curve on the real part of  $Z'$  axis in the high frequencies range corresponds to the equivalent series resistance (ESR) value (also called the solution resistance,  $R_s$ ) and is described as the resistance of both the electrolyte, contact resistance at the active material/current collector interface and the internal resistance of the electrode [8,29]. The Nyquist spectrum of both electrodes can be represented by a modified

Randles circuit [30] also referred to as an equivalent circuit (EQC) with a set of resistors and capacitors as shown in the inset to Fig. 5a. From the figure, the EIS data fitting software (ZFIT) that applies the complex nonlinear least-squares (CNLS) method [31] is used for fitting experimental data with a model which best describes the circuit elements. The equivalent series resistance,  $R_S$  is in series with the constant phase element,  $Q$ . The small semi-circular arc in the high-frequency region to mid-frequency is modelled by a charge transfer resistance  $R_{CT}$  and  $Q$  which is responsible for the ideal capacitance of the samples both connected in parallel to each other.

The high-frequency semicircle to the mid-frequency tail can be represented by the Warburg element  $W$  which is expressed as:

$$W = A/j\omega^{0.5} \quad (7)$$

where  $A$  is the Warburg coefficient,  $\omega$  is the angular frequency and  $n$  is an exponent [32,33].

The impedance of the constant phase element  $Q$ , can be expressed as:

$$Q = 1/T(j\omega)^n \quad (8)$$

where  $T$  is the frequency independent constant with dimensions of  $(F \text{ cm}^{-2})^n$  related to the roughness and pseudocapacitive kinetics of the electrode,  $n$  value varies from -1 to 1 and can be calculated from the slope of the  $\log Z$  versus  $\log f$ . For values of  $n = 0$ ,  $Q$  acts as a pure resistor while for  $n = 1$ ,  $Q$  acts as a pure capacitor and acts as an inductor when  $n = -1$  [34].

For very low frequency values, an ideal electrode produces a vertical line parallel to the imaginary axis with a mass capacitance represented as  $Q$ . The deviation from this ideal behaviour is linked with a leakage resistance  $R_L$  and is placed parallel to the  $C_L$  in the equivalent

circuit.  $C_L$  denotes the pseudocapacitance which arises as a result of the Faradaic charge transfer process [33].

The charge transfer resistance ( $R_{CT}$ ) describes the rate of redox reactions at the electrolyte-electrode interface [35] and this corresponds to the semi-circular arc radius [28]. A lower  $R_{CT}$  value implies a faster ion transport during operation. Therefore, a higher ion transport rate will lead to an enhanced device electrochemical performance. From the experimental data obtained, the arc radius formed in Fig. 5a is smaller for the simonK/GF composite which confirms the faster ion transport. The ESR value from the Nyquist plots improves from 0.55  $\Omega$  for simonK alone to 0.35  $\Omega$  for the simonK/GF composite respectively as read from the intercept of  $Z'$  and this is clearly shown by the inset to Fig. 5a for zoomed-in high to mid frequency part. This is possibly due to the presence of graphene foam in the composite electrode material.

The ESR value obtained from the fitting for simonK and simonK/GF composite is calculated as 0.595  $\Omega$  and 0.368  $\Omega$  respectively. This is seen to be close to the values obtained experimentally and signifies an excellent fit with the experimental data. Thus, it is reasonable to state that the enhancements observed, could be attributed to the better conductivity and favorable electron transfer rate within the composite electrode material. The n-values obtained from the fitting of the Nyquist plots for the simonK and simonK/GF composite were calculated as 0.647 and 0.769 respectively. Thus the results for n indicate a capacitive behavior from the above discussions. This further confirms a successful fitting process on the experimental data obtained from EIS analysis. A summary of the CNLS fitting parameters from the experimental impedance spectra is presented in Table 1.

The stability of the electrode material of supercapacitors is also a very important characteristic for their application as energy storage devices. Fig. 5b shows the continuous galvanostatic charge–discharge cycling of simonK and simonK/GF composite respectively, at  $10 \text{ A g}^{-1}$  current density for 1000 cycles. The stability plot was characterized by little change in the coulombic efficiency obtained from repeated charging and discharging in both materials, which initially increased after a few number of cycles before stabilizing at a higher number of cycles. It is suggested that this increase is as a result of the full exposure of electrolyte ions to some inner sites of the electrode material which were not exposed during the initial cycling stage, and due to the activation of simonK/GF sites which contribute to an increase in capacitance after some initial cycling of the active electrode material [5,14]. The coulombic efficiency of the simonK electrode material after 1000 cycles is recorded at a value of 43.1%. However, for simonK/GF composite, a much more improved and stable coulombic efficiency of 99.7% is recorded after 1000 cycles. This is also an improvement over our earlier report for application of simonK as supercapacitor electrodes [11]. This is an indication that the addition of graphene foam to the simonK matrix has a long-term electrochemical stability and a high degree of charge – discharge reversibility. The excellent pseudocapacitive behavior and high cycling stability can be attributed to the high electrical conductivity and improved specific surface area, allowing rapid and effective ion charge transfer and electron transport.

Since redox reactions also take place during the continuous cycling charge–discharge process, a comparison was made for the CV curves before and after cycling as represented in Fig. 5c to further analyze the cyclic stability of the composite electrode material. Similar CV curves were obtained before and after the 1000<sup>th</sup> cycle with a little shift in the cathodic peak. In other words, both CV curves appear with their usual redox peaks which confirm the electrode stability.

However, a slight reduction in the intensity and observed shift of the peak position is possibly caused by consumption of some of the active sites in the material which leads to some subsequent capacitance loss [28]. Thus, these results show the suitable use of the composite electrode for energy storage applications due to the promising and improving trend of electrochemical properties.

#### **4. Conclusion**

In this paper, we reported an excellent and improved pseudocapacitance behavior of simonK/GF microplatelets synthesized by an in situ hydrothermal technique on nickel foam-graphene (NF-G) current collector as compared to simonK alone. The choice of the NF-G substrate was used based on earlier studies which showed better response when used as a current collector [36]. The simonK/GF composite electrode exhibits an enhanced electrochemical performance due to the presence of the graphene in the simonK matrix and gives a specific capacitance of  $1094 \text{ F g}^{-1}$  at a current density of  $1 \text{ A g}^{-1}$  and a capacitive retention of about 99.7% after 1000 charge–discharge cycles. This shows that these composites are promising electrode materials for energy storage devices.

## **Acknowledgments**

This work is based upon research supported by the South African Research Chairs Initiative (SARChi) of the Department of Science and Technology (DST) and the National Research Foundation (NRF). Any opinion, findings and conclusions or recommendations expressed in this work are those of the authors and the NRF and DST do not accept any liability with regard thereto. D.Y acknowledges the financial support from University of Pretoria and the NRF Doctorate Innovation Fund for his study.

## References

- [1] P. Simon, Y. Gogotsi, Materials for electrochemical capacitors, *Nat. Mater.* 7 (2008) 845–854.
- [2] L. Wang, D. Wang, X.Y. Dong, Z.J. Zhang, X.F. Pei, X.J. Chen, et al., Layered assembly of graphene oxide and Co-Al layered double hydroxide nanosheets as electrode materials for supercapacitors., *Chem. Commun. (Camb)*. 47 (2011) 3556–8.
- [3] Z. Gao, J. Wang, Z. Li, W. Yang, B. Wang, Graphene nanosheet/Ni<sup>2+</sup>/Al<sup>3+</sup> layered double-hydroxide composite as a novel electrode for a supercapacitor, *Chem. Mater.* 23 (2011) 3509–3516.
- [4] J. Memon, J. Sun, D. Meng, W. Ouyang, M.A. Memon, Y. Huang, et al., Synthesis of graphene/Ni–Al layered double hydroxide nanowires and their application as an electrode material for supercapacitors, *J. Mater. Chem. A*. 2 (2014) 5060.
- [5] W. Yang, Z. Gao, J. Wang, J. Ma, M. Zhang, L. Liu, Solvothermal one-step synthesis of Ni-Al layered double hydroxide/carbon nanotube/reduced graphene oxide sheet ternary nanocomposite with ultrahigh capacitance for supercapacitors., *ACS Appl. Mater. Interfaces*. 5 (2013) 5443–5454.
- [6] B. Wang, G.R. Williams, Z. Chang, M. Jiang, J. Liu, X. Lei, et al., Hierarchical NiAl Layered Double Hydroxide/Multiwalled Carbon Nanotube/Nickel Foam Electrodes with Excellent Pseudocapacitive Properties, *ACS Appl. Mater. Interfaces*. 6 (18) (2014) 16304 - 16311.
- [7] P. Chen, G. Shen, Y. Shi, H. Chen, C. Zhou, Preparation and characterization of flexible asymmetric supercapacitors based on transition-metal-oxide nanowire/single-walled carbon nanotube hybrid thin-film, *ACS Nano*. 4 (2010) 4403–4411.
- [8] Z. Fan, J. Yan, T. Wei, L. Zhi, G. Ning, T. Li, et al., Asymmetric Supercapacitors Based on Graphene/MnO<sub>2</sub> and Activated Carbon Nanofiber Electrodes with High Power and Energy Density, *Adv. Funct. Mater.* 21 (2011) 2366–2375.
- [9] M.-Q. Zhao, Q. Zhang, J.-Q. Huang, F. Wei, Hierarchical Nanocomposites Derived from Nanocarbons and Layered Double Hydroxides - Properties, Synthesis, and Applications, *Adv. Funct. Mater.* 22 (2012) 675–694.
- [10] J. Sithole, B.D. Ngom, S. Khamlich, E. Manikanadan, N. Manyala, M.L. Saboungi, et al., Simonkolleite nano-platelets: Synthesis and temperature effect on hydrogen gas sensing properties, *Appl. Surf. Sci.* 258 (2012) 7839–7843.
- [11] S. Khamlich, A. Bello, M. Fabiane, B.D. Ngom, N. Manyala, Hydrothermal synthesis of simonkolleite microplatelets on nickel foam-graphene for electrochemical supercapacitors, *J. Solid State Electrochem.* 17 (2013) 2879–2886.

- [12] F. Hawthorne, E. Sokolova, Simonkollite,  $Zn_5(OH)_8Cl_2(H_2O)$ , a decorated interrupted-sheet structure of the form  $[MO_2]_4$ , *Can. Mineral.* 40 (2002) 939–946.
- [13] K.J. Huang, L. Yan, C.S. Xie, Effect of Surfactants on the Morphologies of ZnO Nanostructures Synthesized by Hydrothermal Method and its Gas Sensitivity to Formaldehyde, in: *Adv. Mater. Res.*, 2011: pp. 628–633.
- [14] L. Zhang, J. Wang, J. Zhu, X. Zhang, K. San Hui, K.N. Hui, 3D porous layered double hydroxides grown on graphene as advanced electrochemical pseudocapacitor materials, *J. Mater. Chem. A*. 1 (2013) 9046.
- [15] T. Long, S. Yin, K. Takabatake, P. Zhnag, T. Sato, Synthesis and Characterization of ZnO Nanorods and Nanodisks from Zinc Chloride Aqueous Solution., *Nanoscale Res. Lett.* 4 (2008) 247–253.
- [16] C. Liu, F. Li, L.-P. Ma, H.-M. Cheng, Advanced materials for energy storage., *Adv. Mater.* 22 (2010) E28–62.
- [17] M. Zhi, C. Xiang, J. Li, M. Li, N. Wu, Nanostructured carbon-metal oxide composite electrodes for supercapacitors: a review., *Nanoscale*. 5 (2013) 72–88.
- [18] W.L. Bragg, The diffraction of short electromagnetic waves by a crystal, in: *Proc. Camb. Philol. Soc.*, 1913: pp. 43–57.
- [19] N.V. Bhat, M.M. Nate, M.B. Kurup, V.A. Bambole, Structural changes in chlorine implanted poly(vinyl alcohol) films, *Nucl. Instruments Methods Phys. Res. Sect. B Beam Interact. with Mater. Atoms.* 262 (2007) 39–45.
- [20] T. Ishikawa, K. Matsumoto, K. Kandori, T. Nakayama, Anion-exchange and thermal change of layered zinc hydroxides formed in the presence of Al(III), *Colloids Surfaces A Physicochem. Eng. Asp.* 293 (2007) 135–145.
- [21] Y. Tao, L. Ruiyi, L. Zaijun, L. Junkang, W. Guangli, G. Zhiquo, A free template strategy for the fabrication of nickel/cobalt double hydroxide microspheres with tunable nanostructure and morphology for high performance supercapacitors, *RSC Adv.* 3 (2013) 19416.
- [22] H. KuanXin, Z. Xiaogang, L. Juan, Preparation and electrochemical capacitance of Me double hydroxides (Me=Co and Ni)/TiO<sub>2</sub> nanotube composites electrode, *Electrochim. Acta.* 51 (2006) 1289–1292.
- [23] J. Yan, Z. Fan, T. Wei, W. Qian, M. Zhang, F. Wei, Fast and reversible surface redox reaction of graphene–MnO<sub>2</sub> composites as supercapacitor electrodes, *Carbon N. Y.* 48 (2010) 3825–3833.

- [24] P. Simon, Y. Gogotsi, B. Dunn, Materials science. Where do batteries end and supercapacitors begin?, *Science*. 343 (2014) 1210–1.
- [25] J.-W. Lang, L.-B. Kong, W.-J. Wu, M. Liu, Y.-C. Luo, L. Kang, A facile approach to the preparation of loose-packed Ni(OH)<sub>2</sub> nanoflake materials for electrochemical capacitors, *J. Solid State Electrochem.* 13 (2008) 333–340.
- [26] J. Wang, Y. Song, Z. Li, Q. Liu, J. Zhou, X. Jing, et al., In Situ Ni/Al Layered Double Hydroxide and Its Electrochemical Capacitance Performance, *Energy & Fuels*. 24 (2010) 6463–6467.
- [27] Z.J. Lao, K. Konstantinov, Y. Tournaire, S.H. Ng, G.X. Wang, H.K. Liu, Synthesis of vanadium pentoxide powders with enhanced surface-area for electrochemical capacitors, *J. Power Sources*. 162 (2006) 1451–1454.
- [28] B. Wang, Q. Liu, Z. Qian, X. Zhang, J. Wang, Z. Li, et al., Two steps in situ structure fabrication of Ni–Al layered double hydroxide on Ni foam and its electrochemical performance for supercapacitors, *J. Power Sources*. 246 (2014) 747–753.
- [29] B.E. Conway, V. Birss, J. Wojtowicz, The role and utilization of pseudocapacitance for energy storage by supercapacitors, *J. Power Sources*. 66 (1997) 1–14.
- [30] J.E.B. Randles, Kinetics of rapid electrode reactions, *Discuss. Faraday Soc.* 1 (1947) 11–19.
- [31] B. Conway, *Electrochemical supercapacitors: Scientific fundamentals and technological applications*, Kluwer Academic Publishers, Plenum Press: New York, 1999.
- [32] Y. Zhou, H. Xu, N. Lachman, M. Ghaffari, S. Wu, Y. Liu, et al., Advanced asymmetric supercapacitor based on conducting polymer and aligned carbon nanotubes with controlled nanomorphology, *Nano Energy*. 9 (2014) 176–185.
- [33] C. Masarapu, H.F. Zeng, K.H. Hung, B. Wei, Effect of Temperature on the Capacitance of Carbon Nanotube Supercapacitors, 3 (2009) 2199–2206.
- [34] H. Guan, L.-Z. Fan, H. Zhang, X. Qu, Polyaniline nanofibers obtained by interfacial polymerization for high-rate supercapacitors, *Electrochim. Acta*. 56 (2010) 964–968.
- [35] M. Sluyters-Rehbach, Impedances of electrochemical systems : Terminology , Nomenclature and Representation PART I : Cells with metal electrodes and liquid solutions, *Pure Appl. Chem.* 66 (1994) 1831–1891.
- [36] D. Momodu, A. Bello, J. Dangbegnon, F. Barzegeer, F. Taghizadeh, A.T.C. Johnson, et al., Solvothermal synthesis of NiAl double hydroxide microspheres on a nickel foam-graphene as an electrode material for pseudo-capacitors, *AIP Adv.* 4 (2014) 097122.

## List of figures

**FIG 1** SEM of; (a,b) simonkolleite at low and higher magnification; (c,d) simonkolleite-graphene foam at low and high magnification (e) simonkolleite and (f) simonkolleite-graphene foam on NF-G.

**FIG 2** (a) N<sub>2</sub> absorption/desorption isotherms; (b) pore size distribution of simonkolleite and simonkolleite-graphene foam composite.

**FIG 3** (a) XRD patterns and (b) FTIR spectra of simonkolleite and simonkolleite-graphene foam composite.

**FIG 4** (a) Cyclic voltammetry (a) nickel foam-graphene, simonkolleite and simonkolleite-graphene foam composite; (b) simonkolleite and (c) simonkolleite-graphene foam grown in situ on NF-G at scan rates of 10 – 100 mV s<sup>-1</sup>; Galvanostatic charge – discharge of (d) simonkolleite and (e) simonkolleite-graphene foam composite measured at current densities of 1 – 10 A g<sup>-1</sup>; (f) specific capacitance of simonkolleite and simonkolleite-graphene foam composite electrode at different current densities calculated from the galvanostatic discharge curves.

**FIG 5** (a) EIS plot of simonkolleite and simonkolleite-graphene foam composite (*insets to the fig. shows the high frequency region zoomed in and a fitted RC circuit related to the sample electrodes respectively*) (b) Dependence of the coulombic efficiency on the charge-discharge cycle number for simonkolleite and simonkolleite-graphene foam on NF-G at a current density of 10 A g<sup>-1</sup>; (c) CV comparison before and after 1000 cycles at a scan rate of 10 mV s<sup>-1</sup> of simonkolleite-graphene foam composite.

## List of tables

**Table 1.** Calculated Values of fitted parameters through CNLS Fitting of the Experimental Impedance Spectra Based on the equivalent circuit shown in the inset to Fig. 5a

## Highlights

- Graphene foam (GF) was grown by atmospheric Chemical Vapor Deposition (AP-CVD)
- In situ solvothermal technique was used to prepare simonkolleite-graphene foam composite (simonK/GF) electrode
- Microscopy results reveal exfoliation of thinner simonK sheets interlaced with sheets of GF
- Presence of active mesopores required for ion transport and improved surface area is seen due to graphene foam addition
- The simonK/GF electrode exhibited improved electrochemical performance compared to simonkolleite electrode alone

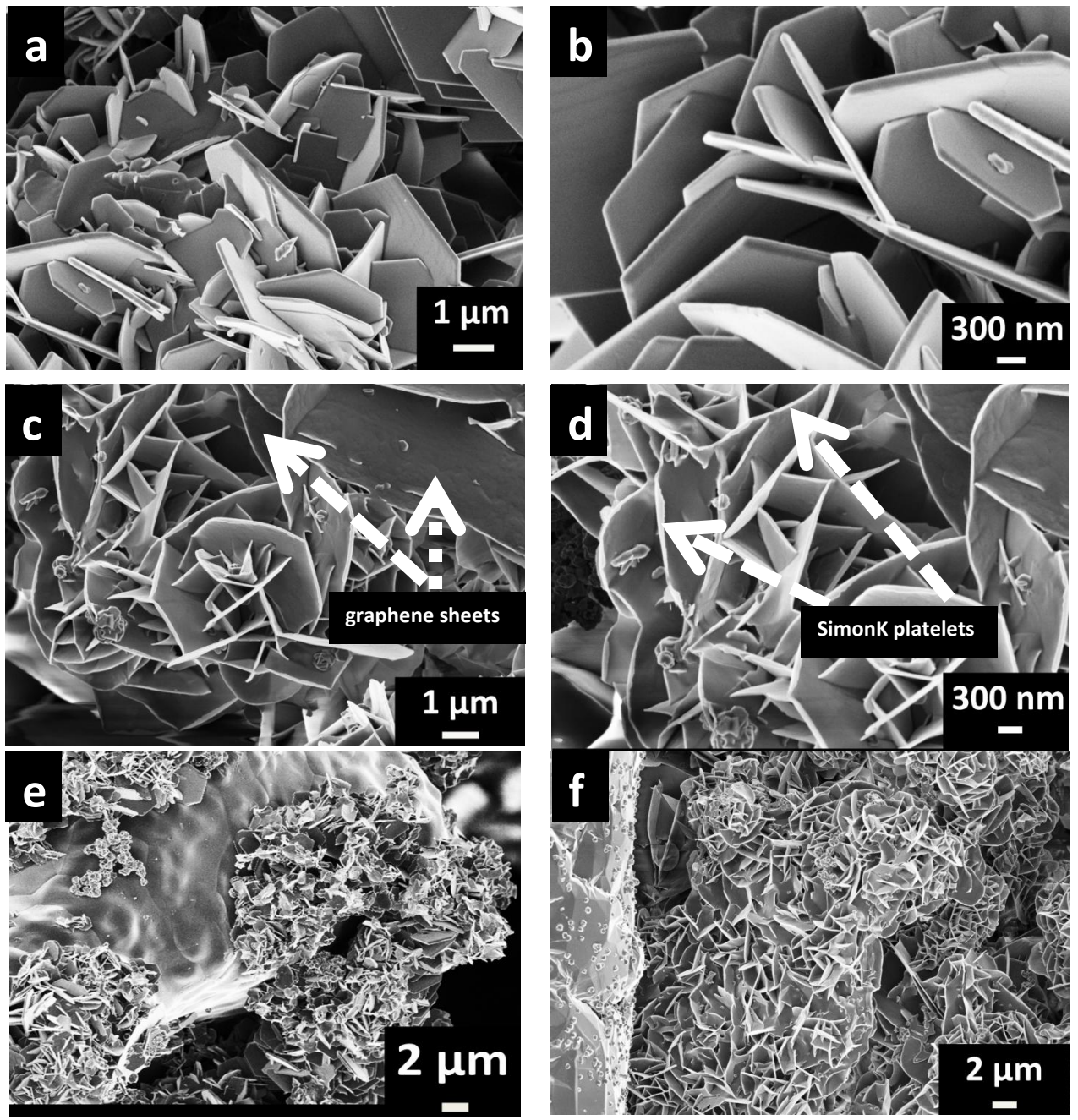


FIG 1

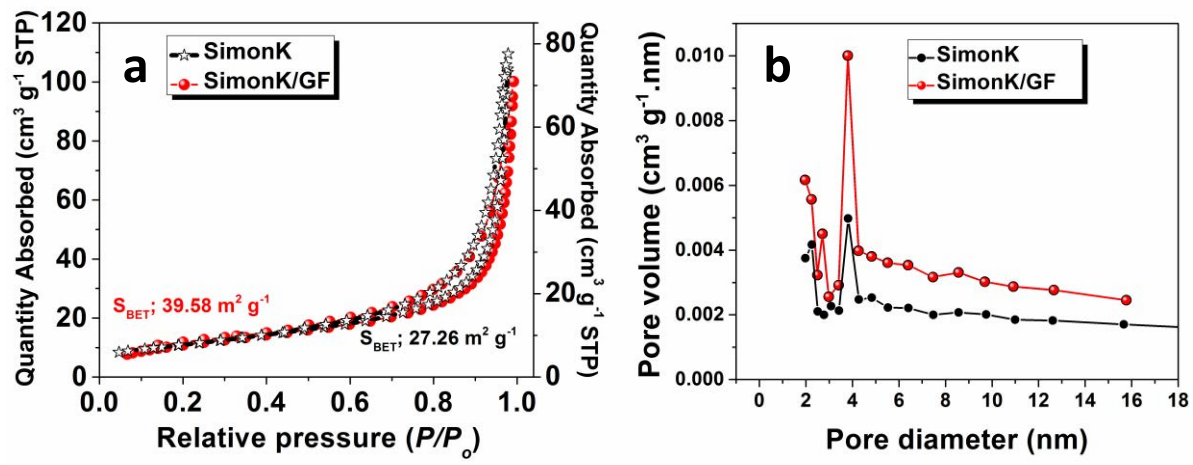


FIG 2

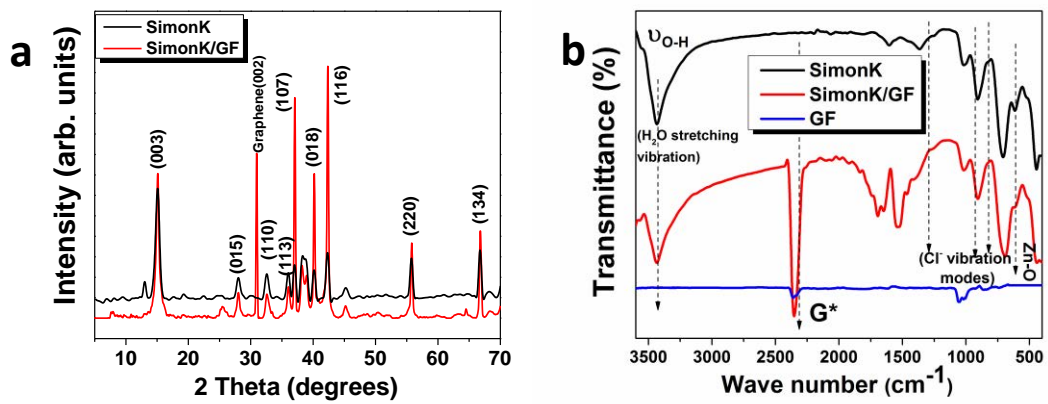


FIG 3

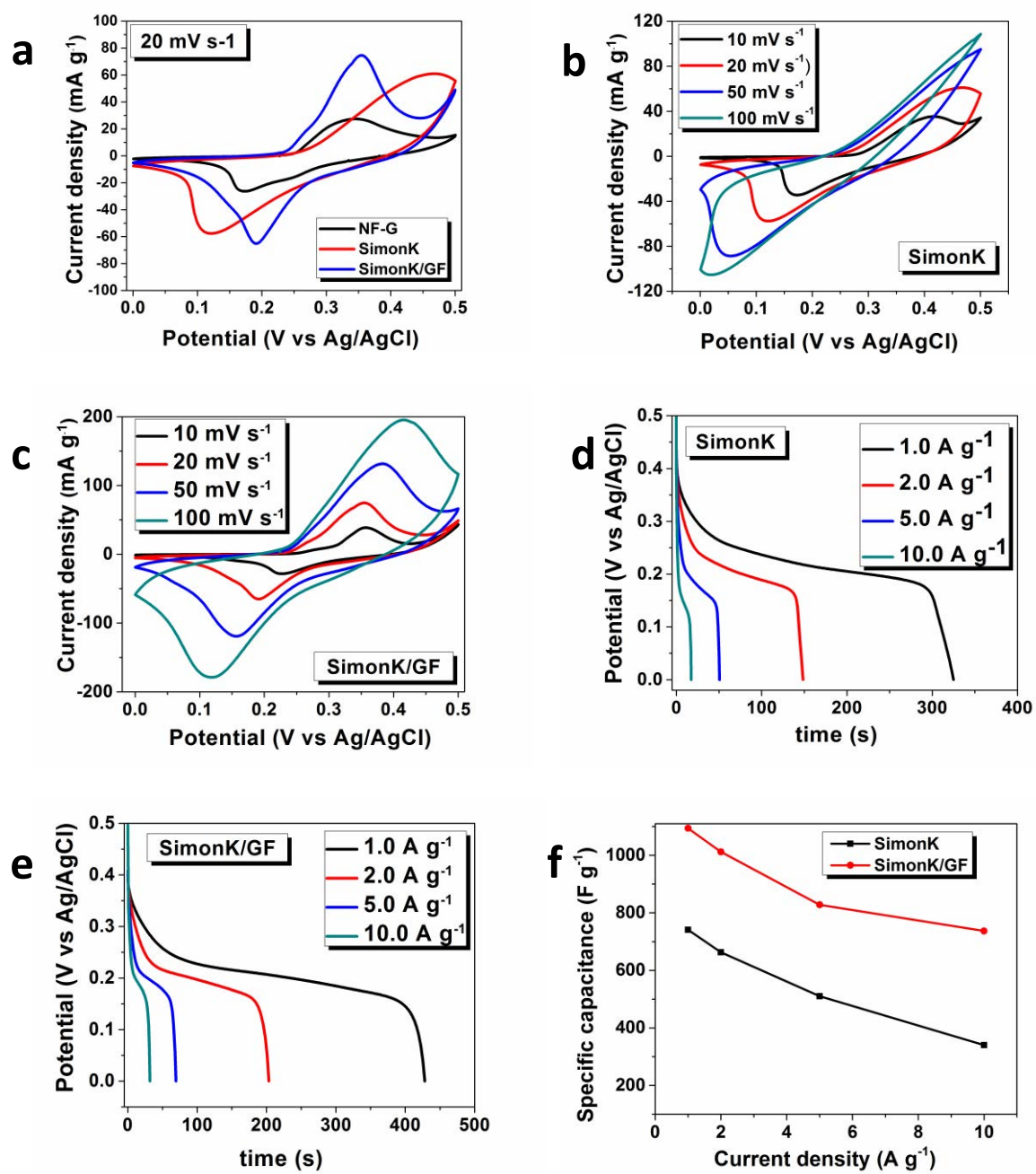


FIG 4

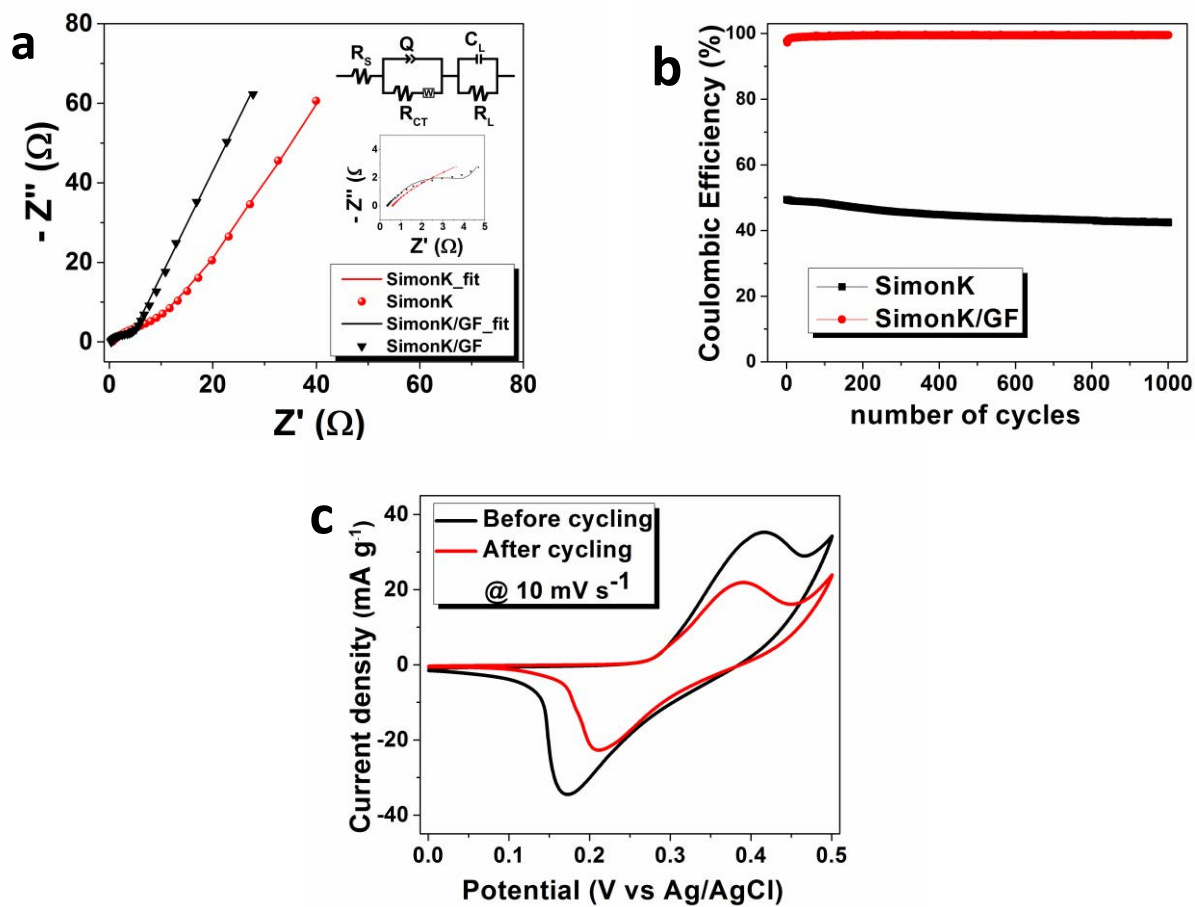


FIG 5

**Table 1.** Calculated Values of fitted parameters through CNLS Fitting of the Experimental Impedance Spectra Based on the equivalent circuit shown in the inset to Fig. 5a

<b>Electrode</b>	<b>R<sub>s</sub></b> <b>(<math>\Omega</math>)</b>	<b>R<sub>CT</sub></b> <b>(<math>\Omega</math>)</b>	<b>C<sub>L</sub></b> <b>(F)</b>	<b>n</b>	<b>Q</b>
<b>SimonK</b>	<b>0.595</b>	<b>9.638</b>	<b>0.350</b>	<b>0.647</b>	<b>0.126</b>
<b>SimonK/GF</b>	<b>0.368</b>	<b>3.942</b>	<b>0.674</b>	<b>0.769</b>	<b>0.014</b>